

Original containing color plates... is a white to black and white

AD-A274 970

2

REPORT DOCUMENTA



Form Approved OMB NO. 0704-0188

|  |  |  |  |   |  |
|--|--|--|--|---|--|
| 1. AGENCY USE ONLY (Leave blank)   |  | 2. REPORT DATE<br>November 30, 1993                      |  | 3. REPORT TYPE AND DATES COVERED<br>Annual, 1 Oct 92 - 31 Sep 93  |  |
| 4. TITLE AND SUBTITLE<br>High Resolution Measurements of Mixing and Reaction Processes in Turbulent Flows (U)  |  |  |  | 5. FUNDING NUMBERS<br>PE - 61102F<br>PR - 2308<br>SA - BS<br>G - AFOSR 89-0541  |  |
| 6. AUTHOR(S)<br>W.J.A. Dahm  |  |  |  | 7. PERFORMING ORGANIZATION(S) AND ADDRESS(ES)<br>Gas Dynamics Laboratories<br>Department of Aerospace Engineering<br>The University of Michigan<br>Ann Arbor, MI 48109-2118 |  |
| 8. SPONSORING ORGANIZATION NAME(S) AND ADDRESS(ES)<br>AFOSR/NA<br>110 Duncan Avenue, Suite B115<br>Bolling AFB, DC 20332-0001  |  |  |  | 9. PERFORMING ORGANIZATION REPORT NUMBER<br>AFOSR-TR-89-0541  |  |
| 10. SPONSORING ORGANIZATION REPORT NUMBER  |  |  |  |   |  |
| 11. SUPPLEMENTARY NOTES  |  |  |  |   |  |
| 12a. DISTRIBUTION / AVAILABILITY STATEMENT<br>Approved for public release; distribution is unlimited   |  |  |  | 12b. DISTRIBUTION CODE  |  |
| 13. ABSTRACT (Maximum: 200 words)<br>Fully-resolved, two-, three-, and four-dimensional, spatio-temporal imaging measurements of the fine structure of conserved scalar mixing in turbulent flows are being used to identify new insights into molecular mixing and develop practical models for turbulent combustion. During the past year, the high wavenumber part of the scalar mixing spectrum has been measured and appears to confirm the Batchelor model. However the cutoff wavenumber is found to lie significantly lower than classical theory suggests. We have also obtained the first measurements of the distribution of dissipation layer separations in turbulent flows. These results show a surprisingly simple and potentially insightful -3 power law scaling for scalar mixing that has not yet been explained. A new strained dissipation and reaction layer (SDRL) model has been developed that relates the chemical state of nonequilibrium reaction chemistry to the mixing state of one or more conserved scalar fields. We have coupled this model with our high resolution Rayleigh imaging measurements to predict combustion species concentration and reaction rate fields in turbulent reacting flows. Results from this model show striking agreement with direct species imaging measurements in turbulent combustion, and allow access to species that cannot be measured directly. This new physically-based formulation appears to unify the previous "flamelet" and "distributed" reaction models within a single model capable of treating even deep nonequilibrium combustion. |  |  |  |   |  |
| 14. SUBJECT TERMS<br>Turbulent Flows; Turbulent Mixing; Turbulent Reacting Flows; Combustion   |  |  |  | 15. NUMBER OF PAGES<br>39   |  |
|  |  |  |  | 16. PRICE CODE  |  |
| 17. SECURITY CLASSIFICATION OF REPORT<br>Unclassified  |  | 18. SECURITY CLASSIFICATION OF THIS PAGE<br>Unclassified |  | 19. SECURITY CLASSIFICATION OF ABSTRACT<br>Unclassified   |  |
|  |  |  |  | 20. LIMITATION OF ABSTRACT<br>UL  |  |

DTIC SELECTED JAN 27 1994

NSN 7540-01-280-5500

44 459

94-02656



Standard Form 298 (890104 Draft) Prescribed by ANSI Std. Z39-18 298-01

94 1 26 109

# DISCLAIMER NOTICE



THIS DOCUMENT IS BEST QUALITY AVAILABLE. THE COPY FURNISHED TO DTIC CONTAINED A SIGNIFICANT NUMBER OF COLOR PAGES WHICH DO NOT REPRODUCE LEGIBLY ON BLACK AND WHITE MICROFICHE.

## 1. Summary of Research Progress

This section summarizes progress made during the reporting period in the understanding and modeling of combustion in turbulent flows.

- A brief introduction and overview of the research program is given in §1.1, outlining the two major areas of current work.
- Section 1.2 summarizes our new strained dissipation and reaction layer model and gives results for the structure of combustion species in turbulent flows. Results to date from this new model show striking agreement with direct species imaging measurements in turbulent combustion, and allow insight into species reaction rate fields in turbulent combustion. These show thin "flamelet-like" OH zones at low nonequilibrium levels, and broad "distributed" OH zones under conditions of deep chemical nonequilibrium. This new physically-based approach appears to unify these two previous disparate combustion concepts within a single model capable of treating even deep nonequilibrium combustion in turbulent flows.
- Following this, §1.3 summarizes results from our measurements of the scaling properties of the scalar dissipation layers which form the basic feature of the molecular mixing process in turbulent flows. In particular, our results appear to verify the  $-1$  power law scaling in the high wavenumber part of the scalar spectrum. However, the cutoff wavenumber for this scaling lies at a significantly lower value than suggested by classical theory. Also, our results show a surprising  $-3$  power law scaling in the distribution of scalar dissipation layer separations that has not yet been explained.

### 1.1 Introduction and Overview

This research program in the Gas Dynamics Laboratories at The University of Michigan consists of a combined experimental and theoretical investigation with the following three major objectives:

- (i) to develop and implement new, high-resolution, multi-dimensional, quantitative, imaging capabilities for obtaining direct experimental measurements of the molecular mixing and chemical reaction processes in turbulent flows,

DTIC QUALITY INSPECTED 8

|                                    |   |
|------------------------------------|---|
| Decision For                       |   |
| DTIC                               | CRA&I <input checked="" type="checkbox"/> |
| DTIC                               | TAB <input type="checkbox"/>              |
| Announced <input type="checkbox"/> |   |
| Justification                      |   |
| By _____                           |   |
| Distribution /                     |   |
| Availability Codes                 |   |
| Dist                               | Avail and/or Special                      |
| A-1                                |   |

- (ii) to use these new measurement techniques to experimentally investigate the essential physical characteristics of molecular mixing and chemical reactions in turbulent flows, and
- (iii) to incorporate results from these new experimental measurements into practical models of the molecular mixing, chemical reaction, and local extinction processes in reacting turbulent flows of interest for air-breathing propulsion systems.

This program is yielding insights into the structure of reacting turbulent flows at the molecular diffusion and chemical reaction scales of the flow. It is based on direct measurements of the fully space- and time-varying fine structure of conserved scalar fields  $\zeta(\mathbf{x},t)$  in nonreacting turbulent flows, and the relation between these and the physical structure of the corresponding chemical species concentration fields  $Y_i(\mathbf{x},t)$  and the associated chemical reaction rate fields  $w_i(\mathbf{x},t)$  in nonequilibrium reacting turbulent flows. This Annual Report summarizes new results obtained during the second year of this work. Basic concepts essential to the approach undertaken here, as well as results from our work to date, are contained in the 1989-91 Final Report and our previous Annual Report. Results have also been described in greater detail in several technical articles appearing in the refereed archival literature<sup>1</sup> and in several monograph

---

<sup>1</sup> see Dahm, Southerland & Buch (1991) *Physics of Fluids A* 3, 1115-1127.  
Tryggvason & Dahm (1990) *Combustion & Flame* 83, 207-220.  
Chang, Dahm & Tryggvason (1991) *Physics of Fluids A* 3, 1300-1311.  
Southerland, Porter, Dahm & Buch (1991) *Physics of Fluids A* 3, 1385-1392.  
Dahm, Su & Southerland (1992) *Physics of Fluids A* 4, 2191-2206.  
Everett, Driscoll, Dahm & Feikema (1993) *Combustion & Flame*, accepted for publ..  
Southerland, Frederiksen, Dahm & Dowling (1993) *Chaos, Solitons & Fractals*, in press.  
Dahm, Tryggvason & Zhuang (1993) *SIAM J. Appl. Math.*, submitted.

articles and conference presentations<sup>2</sup>.

Work in this program is proceeding along two major avenues. The first involves measurements conducted at moderate Reynolds numbers and large Schmidt numbers using a unique, four-dimensional, high-resolution, non-intrusive imaging capability developed under our Phase I effort. These four-dimensional imaging measurements are yielding fully-resolved, giga-byte sized, experimental data volumes of the precise conserved scalar field structure  $\zeta(\mathbf{x}, t)$  on the inner scales of turbulent flows (see Fig. 1). These data are simultaneously resolved in all three space dimensions and in time, allowing direct extraction of the instantaneous scalar energy dissipation rate field  $\nabla\zeta \cdot \nabla\zeta(\mathbf{x}, t)$  and its time evolution. These two fields can be used to deduce the mixing and chemical reaction processes in turbulent reacting flows. Data of this type have previously been conceivable only from large-scale direct numerical simulations (DNS) of the full Navier-Stokes equations, yet these experimental measurements are now possible in real turbulent flows and can reach conditions outside the range of accessibility of such numerical studies. Under our Phase I effort, these measurements were used to show that essentially all of the molecular mixing in turbulent flows occurs in thin, strained, laminar diffusion layers which can be accurately modeled by a simple canonical solution of the Navier-Stokes and

---

<sup>2</sup> see Dahm, Southerland & Buch (1991) Applications of Laser Techniques to Fluid Mechanics, R. Adrian, Ed., Springer Verlag, Berlin.  
Dahm & Buch (1991) Chemical Reactions and Physical Processes in Turbulent Flows, J. Hunt, Ed., Cambridge University Press.  
Buch, Dahm, Dibble, & Barlow (1992) Proceedings of the 24th International Symposium on Combustion, The Combustion Institute, Pittsburgh.  
Dahm (1992) Proceedings of the 13th Symposium on Turbulence, University of Missouri-Rolla, Rolla, MO.  
Dahm (1992) Turbulence and Molecular Processes in Combustion, T. Takeno, Ed., Elsevier.  
Bish, Dahm & Dowling (1993) Proceedings of the 1993 Fall Meeting of the Western States Section of the Combustion Institute, The Combustion Institute, Pittsburgh.  
Bish & Dahm (1993) 25th International Symposium on Combustion, submitted.  
Su & Dahm (1993) AIAA 25th Fluid Dynamics Meeting, submitted.  
Southerland & Dahm (1993) AIAA 25th Fluid Dynamics Meeting, submitted.  
Frederiksen & Dahm (1993) AIAA 25th Fluid Dynamics Meeting, submitted.  
Bish & Dahm (1993) AIAA 32nd Aerospace Sciences Meeting, submitted.  
Su & Dahm (1993) AIAA 32nd Aerospace Sciences Meeting, submitted.  
Southerland & Dahm (1993) AIAA 32nd Aerospace Sciences Meeting, submitted.  
Suresh, Dahm & Tryggvason (1993) AIAA 32nd Aerospace Sciences Meeting, submitted.

conserved scalar transport equations. Under the present Phase II effort, the larger scale topology and scaling properties of these dissipation layers are being investigated to develop a complete model of the mixing process.

Complementing these studies of molecular mixing in turbulent flows, a second major effort of our work involves highly-resolved, multi-dimensional imaging measurements of  $Sc = 1$  conserved scalar mixing in gaseous turbulent flows. As is the case in our large  $Sc$  measurements, the highly resolved nature of the measurements, together with the very high signal quality achieved, permits direct differentiation of the data to allow accurate evaluation of derivatives involved in the scalar gradient field  $\nabla\zeta(\mathbf{x},t)$ . This yields the structure of scalar energy dissipation rate field, permitting highly detailed analysis of the structure of chemical reactions in nonequilibrium combustion processes occurring in turbulent flows. The local instantaneous thermochemical state of the reacting turbulent flow can be specified from a two-parameter nonequilibrium formulation in terms of the local conserved scalar and scalar dissipation rate values. This procedure is used to examine the reaction zone structure in turbulent flames under varying degrees of chemical nonequilibrium. These measurements are providing a previously inaccessible level of detailed information about the structure of combustion processes in turbulent flows. Results obtained permit the first direct view into the structure of the species chemical reaction rate fields  $w_i(\mathbf{x},t)$  in reactive turbulent flows under various degrees of chemical nonequilibrium.

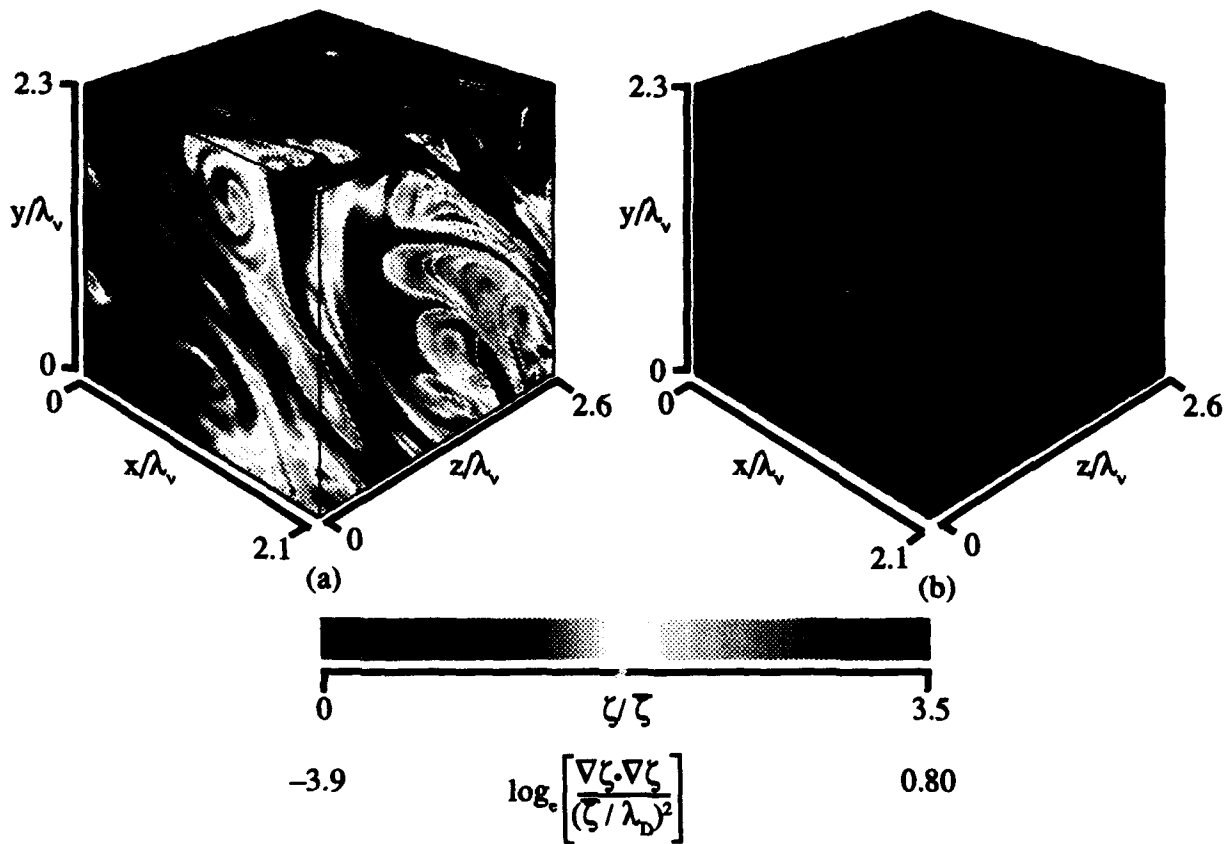


Fig. 1. Experimental data detailing the fluid mixing process at each of over 16 million points in a small three-dimensional spatial data volume taken from a four-dimensional spatio-temporal data space consisting of over 3 billion individual data points obtained in the self-similar far field of an axisymmetric turbulent jet. The volume dimensions are given in terms of the finest velocity gradient lengthscale  $\lambda_v$ , proportional to the classical Kolmogorov scale. Shown are: (a) the conserved scalar concentration field  $\zeta(\mathbf{x}, t)$ , and (b) the associated scalar energy dissipation rate  $(\text{ReSc})^{-1} \nabla \zeta \cdot \nabla \zeta(\mathbf{x}, t)$ . Note the highly convoluted layers in the dissipation field, created by the continual stretching and folding action of the three-dimensional time-varying flow field. For the case shown,  $\text{Re} \approx 3700$  and  $(\text{ReSc}) \approx 8 \times 10^6$ .

## 1.2 Non-Equilibrium Structure of Turbulent Combustion

This section summarizes our development of a new physically-based model for treating the coupling between molecular mixing and combustion chemistry in turbulent flows. It is based on structure of the scalar dissipation field obtained from our earlier measurements.

**1.2.1 Background.** Over the past several years, our results and others from conserved scalar imaging measurements in nonreacting turbulent flows [1-6] as well as direct numerical simulations (DNS) of passive scalar mixing in turbulent flows [7-11] have shown that, whereas the underlying hydrodynamics of turbulent flows are quite complex, the structure of scalar mixing in such flows is considerably simpler. In particular, while the instantaneous vorticity field is a complex arrangement of line-like, sheet-like, and intermediate structures, for dynamically passive conserved scalar fields  $\zeta(\mathbf{x},t)$  with Schmidt numbers  $(\nu/D_\zeta)$  of unity or larger, essentially all of the instantaneous scalar energy dissipation rate field  $\chi(\mathbf{x},t) \equiv (ReSc)^{-1} \nabla \zeta \cdot \nabla \zeta(\mathbf{x},t)$  is organized into locally one-dimensional layer-like dissipation sheets. Examples of these dissipation layers can be seen in Fig. 1, from Buch & Dahm [4]. The dynamics of the strain-diffusion competition involved in scalar mixing, which leads to the inexorable formation of such layer-like scalar dissipation structures and to the exclusion of the complementary line-like dissipative structures found in the underlying vorticity field, are discussed in detail in Ref. [4]. These layer-like scalar dissipation sheets are simply the three-dimensional analog of the localized dissipation "shocks" that arise naturally from the advection-diffusion balance in high Reynolds number solutions to the diffusive Burgers' equation.

In reacting turbulent flows, the advection-diffusion balance that leads to the formation of these ubiquitous scalar dissipation layers is present as well. In the presence of combustion heat release, the individual chemical species diffusivities  $D_i$  vary with local temperature, however the hydrodynamic viscosity  $\nu$  scales in essentially the same way and thus  $Sc$  remains essentially constant near unity. This leads to a change in the lengthscale characterizing the thickness of these layer-like dissipation structures, but does not alter the basic strain-diffusion competition that establishes these structures. Additionally, the underlying strain rate and vorticity fields are modified by the fluid expansion due

to combustion heat release, and the baroclinic vorticity due to the interaction of density gradients with the hydrostatic pressure gradient (buoyancy) and with local hydrodynamic pressure gradients. However for heat release values typical of hydrocarbon combustion, the local velocity gradients leading to formation and preservation of these dissipation sheets remain dominant in turbulent flows with combustion as well. Recent results from scalar imaging measurements by Long [12] as well as DNS computations appear to confirm that these layer-like scalar dissipation structures remain present even in turbulent flows undergoing highly exothermic combustion reactions.

The implications of this fundamentally layer-like structure of scalar mixing in turbulent flows are substantial, especially for turbulent combustion. As noted above, these dissipation layers result entirely for hydrodynamical reasons. Thus *all* conserved scalar quantities with  $Sc \geq 1$  must have their scalar energy dissipation concentrated in such locally one-dimensional layer-like structures. This will be true irrespective of whether the scalar is a passive physical quantity (such as an inert dye or gaseous tracer), or a more abstract quantity formed from the concentrations of various chemical species evolving in the flow (such as any of various mixture fraction variables). Thus the dissipation fields associated with all conserved scalar mixture fractions must *also* remain manifestly layer-like, and since this is a consequence solely of the hydrodynamics of scalar mixing, this must remain true irrespective of the degree of chemical nonequilibrium to which the various constituent chemical species fields are subjected – the presence of locally one-dimensional dissipation layers in mixture fraction fields is entirely independent of the chemical state in the flow. As a consequence, any model relating the combustion chemistry in a turbulent flow to the underlying fluid dynamics must, at a minimum, recover this layer-like dissipation structure once the resulting reactive species concentrations are formed into mixture fraction variables. Conversely, the inherently layer-like structure of the dissipation rate fields associated with mixture fraction variables in turbulent flows provides a rigorous starting point for models of nonequilibrium chemistry in turbulent flows.

**1.2.2 The Strained Dissipation and Reaction Layer Formulation.** The ubiquitous scalar energy dissipation layers noted above allow for a physically-based formulation that relates the mixing state of one or more conserved scalars

by the underlying turbulent flow to the chemical state of nonequilibrium combustion occurring within the flow. This approach begins by noting that any conserved scalar mixture fraction variable  $\zeta_i$  can be written as a linear sum over the chemical species fields  $Y_j(\mathbf{x}, t)$  as

$$\zeta_i(\mathbf{x}, t) = \sum_{j=1}^N a_{i,j} Y_j(\mathbf{x}, t) \quad i = 1, 2, \dots, m \quad (1)$$

where  $N$  is the number of chemical species and  $m$  the number of elements involved in the chemical system. Each of the  $m$  conserved scalars  $\zeta_i$  must satisfy the conservative advection-diffusion equation

$$\frac{\partial \zeta_i}{\partial t} + \mathbf{u} \cdot \nabla \zeta_i - \frac{1}{\rho} \nabla \cdot (\rho D_{\zeta_i} \nabla \zeta_i) = 0. \quad (2)$$

Owing to the locally one-dimensional state of the scalar field within any given dissipation layer, as discussed in §2 (see Fig. 1), derivatives of  $\zeta_i$  along the local layer-normal coordinate  $n$  far exceed those along the layer. Thus (2) above reduces to the locally parabolized form

$$\frac{\partial \zeta_i}{\partial t} - \varepsilon(t)n \frac{\partial \zeta_i}{\partial n} - \frac{1}{\rho} \frac{\partial}{\partial n} \cdot \left( \rho D_{\zeta_i} \frac{\partial \zeta_i}{\partial n} \right) = 0 \quad (3)$$

where  $\varepsilon(t)$  is the local time-varying strain rate along the layer-normal direction resulting from the local linear expansion of the velocity field  $\mathbf{u}(\mathbf{x}, t)$ . As is evident in Fig. 1, in general the scalar dissipation layers in turbulent flows do not involve pure fuel or pure air on either side of the layer. Instead the correct *local* boundary conditions for (3) can be expressed as

$$\zeta_i \rightarrow \zeta_i^\pm \quad \text{as } n \rightarrow \pm\infty \quad (4)$$

where the appropriate  $\zeta_i^\pm$  typically vary slowly along the layer. Practical implementation of these boundary conditions will be dealt with below. We will first examine the implications of this local one-dimensionality in the scalar field for the chemical species fields  $Y_j(\mathbf{x}, t)$ .

Replacing  $\zeta_i$  in (3) with its definition in terms of the various chemical species concentration fields in (1), and recalling that the  $a_{i,j}$  are constants, gives

$$\begin{pmatrix} a_{1,1} & a_{1,2} & \cdots & a_{1,N} \\ a_{2,1} & a_{2,2} & \cdots & a_{2,N} \\ \vdots & \vdots & \ddots & \vdots \\ a_{m,1} & a_{m,2} & \cdots & a_{m,N} \end{pmatrix} \begin{pmatrix} L[Y_1(\mathbf{x},t)] \\ L[Y_2(\mathbf{x},t)] \\ \vdots \\ L[Y_N(\mathbf{x},t)] \end{pmatrix} = \begin{pmatrix} 0 \\ 0 \\ \vdots \\ 0 \end{pmatrix} \quad (5)$$

where

$$L[Y_j(\mathbf{x},t)] \equiv \left[ \frac{\partial Y_j}{\partial t} - \epsilon(t)n \frac{\partial Y_j}{\partial n} - \frac{1}{\rho} \frac{\partial}{\partial n} \cdot \left( \rho D_{\zeta_i} \frac{\partial Y_j}{\partial n} \right) - \dot{w}_j / \rho \right]. \quad (6)$$

Here we have also introduced the requirement that, since the  $\zeta_i$  are conserved, the weighted chemical species reaction rate terms  $w_j(\mathbf{x},t)$  must sum to zero as

$$\sum_{j=1}^N a_{i,j} \dot{w}_j(\mathbf{x},t) \equiv 0. \quad (7)$$

We now want to consider the implications of (5) - (7) for the structure of the  $Y_j(\mathbf{x},t)$  fields. Briefly, we will argue that these constraints together require that the only physically realizable solution is the trivial case  $L[Y_j(\mathbf{x},t)] \equiv 0$ , in which case the species conservation equations satisfy locally one-dimensional advection-diffusion-reaction equations within each dissipation layer. In effect, we are arguing from precisely the opposite point of view from that usually taken in deriving the classical "flamelet" model. In deriving the flamelet model, conditions are assumed for which the flamelet is thin, and the species transport equations then formally reduce to locally one-dimensional equations which, in turn, dictate a locally one-dimensional structure in the mixture fraction fields  $\zeta_i(\mathbf{x},t)$ . However, the conditions under which the requisite thin flamelet assumption actually holds are so restrictive as to render the resulting classical flamelet model useful only for small equilibrium departures. Here, we take exactly the opposite point of view. We begin with the physical observation from §2 that the mixture fraction fields  $\zeta_i(\mathbf{x},t)$  in turbulent flows must be locally one-dimensional, and argue that this requires the constituent chemical species fields  $Y_j(\mathbf{x},t)$  to also be locally one-dimensional. (It will be seen below that, unlike the flamelet model, the resulting one-dimensionality in this case does not demand thin "flamelet-like"  $Y_j(\mathbf{x},t)$  fields.) That argument for one-dimensionality in the  $Y_j(\mathbf{x},t)$  fields is complete if  $L[Y_j(\mathbf{x},t)] \equiv 0$  is the only physically realizable solution to (5) - (7). There are three key physical requirements that we argue demand this trivial solution in (5).

- (i) Note that all the  $a_{ij} \geq 0$  in (5), since from (1) each mixture fraction  $\zeta_i$  is simply a sum over all the chemical species  $Y_j$  of their contributions to the tally of each element  $i$ . Thus, owing to the fact that all the  $a_{ij}$ 's have the same sign, the zero sums in (5) can only result from either the trivial solution  $L[Y_j(\mathbf{x}, t)] \equiv 0$ , or else from a fortuitous cancellation of positive and negative  $L[Y_j(\mathbf{x}, t)]$ 's. If the latter is the case, then this cancellation would need to be preserved for each of the  $m$  sums corresponding to the elements  $i = 1, 2, \dots, m$  for the single set of species fields  $Y_j(\mathbf{x}, t)$ .
- (ii) Since typically  $N \gg m$ , there are combinations of the  $L[Y_j(\mathbf{x}, t)]$ 's that will produce these  $m$  zero sums in (i) above, however each of these combinations imposes specific relations between the various  $Y_j(\mathbf{x}, t)$  fields. The restricted  $Y_j(\mathbf{x}, t)$  fields necessary to preserve these  $m$  zero sums would, at the same time, need to be consistent with the kinetics associated with the resulting reaction rate terms. In other words, each of the combinations of the  $Y_j(\mathbf{x}, t)$  fields that satisfies the required cancellation of  $L[Y_j(\mathbf{x}, t)]$ 's corresponds to a set of net elementary reaction rates  $w_j(\mathbf{x}, t)$ . However the resulting  $w_j(\mathbf{x}, t)$  fields must at the same time preserve the zero sum in (7). This would, at a minimum, greatly reduce the set of  $L[Y_j(\mathbf{x}, t)]$ 's simultaneously consistent with both (5) and (7).
- (iii) Lastly, the zero sums in (5) and (7) must be preserved for *all* possible chemical systems, not merely any particular reaction set under consideration. No features of the reaction kinetics specific to any one chemical system can be invoked to satisfy the relations among the  $Y_j(\mathbf{x}, t)$  fields necessary to achieve cancellation of positive and negative  $L[Y_j(\mathbf{x}, t)]$ 's in (5), while at the same time preserving the additional zero sum in (7) for the resulting elementary reaction rates. In other words, the layer-like structure in the scalar dissipation field as expressed by (5) - (7) must be recovered for *every conceivable* elementary chemical system that could hypothetically occur.

Each one of these three observations places strong constraints on the  $Y_j(\mathbf{x}, t)$  fields. The fact that all three of these requirements must be simultaneously met by the coupled  $Y_j(\mathbf{x}, t)$  fields suggests a set of constraints collectively so restrictive as to be physically unrealizable. We therefore hypothesize that the set of simultaneous conditions under which (5) can have a non-trivial solution are mutually exclusive, and that the only physically realizable solution is the trivial case  $L[Y_j(\mathbf{x}, t)] \equiv 0$  for each  $j$ , namely

$$\frac{\partial Y_j}{\partial t} - \epsilon(t)n \frac{\partial Y_j}{\partial n} - \frac{1}{\rho} \frac{\partial}{\partial n} \cdot \left( \rho D_{\zeta_i} \frac{\partial Y_j}{\partial n} \right) = \dot{w}_j / \rho. \quad (8)$$

In other words, the one-dimensionality of the local conserved scalar field across each of these strained dissipation layers implies a locally one-dimensional structure for the underlying chemical species fields within the layer. However, owing to the *local* boundary conditions on (8), this does *not* imply that the resulting  $Y_j(\mathbf{x}, t)$  fields must be layer-like, as will be seen from the results in §4.

As noted in (4), these locally one-dimensional strained dissipation and reaction layers are in general not between pure fuel and air. Instead, the appropriate local boundary conditions on (8) are

$$Y_j \rightarrow Y_j^\pm \quad \text{as } n \rightarrow \pm\infty. \quad (9)$$

Solutions  $Y_j(n, t; \epsilon, Y_j^+, Y_j^-)$  to (8) are thus parametrized by the strain rate  $\epsilon(t)$  and the boundary values  $Y_j^\pm$ . In practice, specification of the appropriate *local* boundary conditions for these one-dimensional advection-diffusion-reaction equations within any given dissipation layer is a non-trivial matter. For the moment, it should be noted that the  $(n, \epsilon)$  dependence in (8) can of course be equivalently replaced with  $(\zeta, \chi)$  from the corresponding conserved scalar solution in (3) to yield the classical "flamelet" equations, though the physical assumptions leading to these two equations are quite different, as are the boundary conditions. Specification of the *correct* local boundary conditions for the flamelet equation is equally difficult, though usually pure fuel and air conditions corresponding to  $\zeta^\pm = (0, 1)$  are specified.

Putting the discussion of boundary conditions aside for the moment, it is appropriate first to comment on the similarities and differences between the present strained dissipation and reaction layer (SDRL) model, and the classical flamelet model, since both arrive at the same governing equations. The SDRL formulation above is a consequence of the one-dimensionality of any conserved scalar variable across the locally layer-like structures seen to dominate scalar energy dissipation rate fields in turbulent flows. The formulation, in this sense, is based entirely on hydrodynamical arguments, and makes no statements about thinness of reaction zones, or places any other requirements on the reaction chemistry. The flamelet model [13], on the other hand, is derived explicitly on the basis of a presumed one-dimensionality in the chemical species fields under

conditions for which the flamelet is "thin" relative to the dissipation scales. This thinness requirement is expressed in various flamelet implementations either as a requirement that variations in the scalar dissipation within the reaction zone must be negligible [13-15], or else that these variations can be modeled via some presumed function such as  $\chi \sim \zeta^p$  [16] or the self-similar solution of the scalar transport equation (3) for free stream boundary conditions [17].

The latter class of flamelet models is most closely related to the present approach, though the thinness requirement to which these are subject is not a constraint here. Moreover the appropriate *local* boundary conditions in (9) for the one-dimensional advection-diffusion-reaction equations within any given dissipation layer differ fundamentally from classical flamelet models. Instead, these correspond to the mass fraction values  $Y_j^\pm$  between neighboring dissipation layers. In practice, the information required to specify the correct  $Y_j^\pm$  will rarely be available. However, the physical nature of the approach developed here allows some insight into how these boundary conditions can be simplified. In particular, we note that the mapping from  $(\zeta, \chi)$  to the strain rate  $\epsilon$ , where

$$\epsilon = 2\pi D \left[ \frac{\nabla \zeta \cdot \nabla \zeta}{(\zeta^+ - \zeta^-)^2} \right] \exp 2 \left\{ \operatorname{erf}^{-1} \left[ \frac{\zeta - \frac{1}{2}(\zeta^+ + \zeta^-)}{\frac{1}{2}(\zeta^+ - \zeta^-)} \right] \right\}^2 \cdot f(\zeta) \quad (10)$$

is very sensitive to the conserved scalar boundary values  $\zeta^+$  and  $\zeta^-$  in (4). Since the strain rate drives the local molecular mixing rate and thus plays a dominant role in setting the depth of nonequilibrium chemistry, it is of primary importance to account for the scalar boundary values properly. In comparison with  $\zeta^+$  and  $\zeta^-$ , the corresponding chemical species boundary values  $Y_j^+$  and  $Y_j^-$  would appear to have less of an effect on the nonequilibrium levels within the layer, since these influence the reaction progress only indirectly. The local departures from chemical equilibrium in each of the species concentrations will therefore be determined principally by the local scalar value  $\zeta$  and the *correct* local strain rate  $\epsilon(\zeta, \chi; \zeta^+, \zeta^-)$ . A direct test of this hypothesis for simplifying the local boundary conditions must await results of a numerical study currently underway; here we will assume that, for a given scalar value  $\zeta$ , the local  $Y_j$  may be determined relatively accurately by correctly accounting the scalar boundary values  $\zeta^+$  and  $\zeta^-$ , which can be readily estimated from two-point statistics of the

scalar field in turbulent flows, and retaining the species boundary values  $Y_j^+$  and  $Y_j^-$  at their free stream values.

**1.2.3 Application to Turbulent Jet Flames.** We have applied this strained dissipation and reaction layer formulation to examine variations in the structure of chemical species concentration and reaction rate fields for increasing degrees of chemical nonequilibrium in a turbulent jet diffusion flame. The results obtained are based on imaging measurements of conserved scalar fields obtained in the corresponding nonreacting flow. The experimental technique has been described in detail elsewhere [4-6]. Briefly, these conserved scalar imaging measurements were made in the self-similar far field of an axisymmetric coflowing turbulent jet. The flow was established in the 30 cm  $\times$  30 cm  $\times$  200 cm test section of the forced draft vertical tunnel with free stream velocity  $U_\infty$  by issuing a jet of undiluted technical grade propane with momentum flux  $J_0$  through a 7.7 mm diameter nozzle. The beam from a 300 mJ/pulse Nd:YAG laser was doubled to 532 nm and formed into a thin sheet passing through the flow. The  $1/e$  laser sheet thickness was measured as 230  $\mu$ m. Rayleigh scattered light from this sheet was imaged onto a 14-bit, slow-scanned, cooled, nonintensified imaging array. The array was sampled in a 256  $\times$  512  $\times$  8-bit format, with each element measuring 23  $\mu$ m  $\times$  23  $\mu$ m. The imaging optics were arranged to give a 1:1 image ratio, with the array output giving the Rayleigh signal integrated over the 10 ns laser pulse duration. The measurement location was centered 39 nozzle diameters downstream of the jet exit at a local outer-scale Reynolds number  $Re \approx 14,000$ . The spatial and temporal resolution achieved were sufficient to distinguish the smallest spatial and temporal scales in the scalar field. Reference measurements with pure air in the test section gave the laser sheet intensity distribution and allowed the effects of non-uniformities in the laser sheet to be largely removed from the data. The Rayleigh signal at each point was then converted to the instantaneous value of the propane mass fraction, yielding a *generic*  $Sc \approx 1$  conserved scalar field  $\zeta(\mathbf{x}, t)$  in the turbulent flow. The structure of the scalar energy dissipation rate field  $\nabla\zeta \cdot \nabla\zeta(\mathbf{x}, t)$  was obtained from the measured  $\zeta(\mathbf{x}, t)$  data using linear central differences on a 3  $\times$  3 template centered on each data point.

Figure 1a shows a typical 256  $\times$  512 data plane of the instantaneous conserved scalar field  $\zeta(\mathbf{x}, t)$ . The 256 different colors denote ranges of

conserved scalar values as indicated, with pure blue beginning at  $\zeta(\mathbf{x}, t) = 0$ , corresponding to pure air, and increasing uniformly to pure red denoting the highest conserved scalar values in the data. The jet centerline runs down the right edge of the plane, and the axes indicate the spatial extent in terms of the local strain-limited scalar gradient lengthscale  $\lambda_D$ . Derivatives of the measured conserved scalar field give the projection of the true three-dimensional scalar gradient vector  $\nabla\zeta(\mathbf{x}, t)$  into the plane. Figure 1b shows the logarithm of the corresponding scalar dissipation rate field formed from this projection,  $\log_e \nabla\zeta \cdot \nabla\zeta(\mathbf{x}, t)$ . The 256 different colors denote the local scalar dissipation rate, with black beginning at  $\nabla\zeta \cdot \nabla\zeta = 0$ , and pure blue through pure red denoting logarithmically increasing dissipation rates.

The local outer variables  $u(x)$  and  $\delta(x)$ , and the mass fraction-based conserved scalar field  $\zeta(\mathbf{x}, t)$ , in the far field of axisymmetric turbulent jets follow self-similar scalings with downstream location  $x$ . Since these scalings produce a Reynolds number that remains constant with increasing downstream distance, measurements such as those in Fig. 1 can be rescaled to map the instantaneous scalar and dissipation rate fields to any  $x$ -location in the self-similar far field of the flow. A given set of chemical reactions occurring in this conserved scalar field would then correspond to a turbulent jet diffusion flame of length  $L$ , where the flame tip is taken to occur at the  $x$ -location for which the maximum conserved scalar value achieves stoichiometry for the fuel and oxidizer combination being considered. The mass fraction and reaction rate fields for any chemical species in this flame can then be constructed from the local values of the scalar and dissipation rate fields using the steady strained dissipation and reaction layer formulation. To do this we use a library for hydrogen-air chemistry in steady, one-dimensional, strained dissipation and reaction layers, generated from numerical calculations supplied by J.-Y. Chen using a subset of the Miller & Bowman [18] kinetic mechanism.

Results are presented for the OH mass fraction and reaction rate fields at various downstream locations for three jet flames corresponding to increasing degrees of chemical nonequilibrium. The conditions for each case considered are shown in Fig. 2, where the depth of nonequilibrium is indicated relative to the flame blowout limit for an unpiloted hydrogen-air turbulent jet diffusion flame. The three cases each have the same far field Reynolds number ( $Re =$

14,000), but correspond to conditions in the flame ranging from near equilibrium (Case 1) to moderate nonequilibrium (Case 2) to deep nonequilibrium (Case 3). With a characteristic temperature of roughly 1800 K, and with  $\nu \sim T^{1.5}$ , a cold-flow Reynolds number of 210,000 in Fig. 2 produces a hot-flow conserved scalar field consistent with the  $Re = 14,000$  measurements in Fig. 1. All results presented below are constructed via the SDRL formulation outlined in §3 using the conserved scalar and scalar dissipation fields in Fig. 1, with a uniform rescaling of these  $\zeta$  and  $\chi$  fields mapping them to any  $x/L$  location for any of the three cases considered. Relative local strain rates for each of the three cases and each of the four downstream locations at which results are presented are given below.

| $x/L$ | Case 1            | Case 2 | Case 3 |
|-------|-------------------|--------|--------|
| 0.25  | 10 ( $10^{-5}$ )  | 1      | 10     |
| 0.50  | 2.5 ( $10^{-5}$ ) | 0.25   | 2.5    |
| 0.75  | 1.1 ( $10^{-5}$ ) | 0.11   | 1.1    |
| 1.00  | 0.6 ( $10^{-5}$ ) | 0.06   | 0.6    |

Table 1. Relative strain rates at each of the four downstream locations and each of the three cases identified in Fig. 2 for which results are shown.

In Fig. 3 we compare the resulting OH mass fraction fields  $Y_{OH}(x,t)$  at  $x/L = 0.25$  for each of the three cases. (Color bars identifying quantitative values for each case are given in Figs. 7-9.) Notice that at this location in the flame, the SDRL formulation produces thin layer-like OH fields for the near-equilibrium conditions in Case 1. The OH layer at these conditions is relatively straight and aligned with the downstream direction, and lies well off the jet centerline. Overall, the resulting OH field for Case 1 is strikingly similar to OH PLIF measurements at small  $x/L$  locations in turbulent jet diffusion flames under conditions of relatively weak nonequilibrium [19, 20]. By comparison, in Case 2 the strain rates at this location are significantly higher (see Table 1), and the SDRL formulation produces considerably broader and more diffuse structures in the OH mass fraction field, with little remaining evidence of the thin layer-like OH zones seen for Case 1. This is also consistent with direct OH PLIF imaging measurements in turbulent jet diffusion flames. For Case 3, the strain rates at

this  $x/L = 0.25$  location are so high that local extinction of the reactions occurs throughout much of the flow, as evidenced by the zero OH values coincident with the high dissipation rates in Fig. 1. The remaining OH zones evident in Case 3 are completely broad and distributed, and show no remaining evidence of the layer-like structure in the underlying scalar dissipation rate field. The corresponding OH reaction rate fields  $w_{OH}(x,t)$  for each of these three cases are shown in Fig. 4.

Moving to a location further downstream in the flame, Fig. 5 shows the OH mass fraction fields that result from the SDRL formulation at  $x/L = 0.50$  for each of the same three flows. A similar transition from thin, layer-like OH mass fraction fields at conditions near chemical equilibrium to broad, distributed OH zones with increasing depth of nonequilibrium, can be seen in the results obtained. There again is a striking resemblance of the OH fields that result for each of these three cases with the basic features of OH PLIF images obtained from direct measurements in turbulent jet diffusion flames under conditions of increasing chemical nonequilibrium [19, 20]. The OH reaction rate fields corresponding to each of the fields in Fig. 5 are shown in Fig. 6. Notice that the thin layer-like reaction rate field that results near equilibrium in Case 1 (see also Ref. [5]) becomes more diffuse with increasing chemical nonequilibrium, leading to a broad and distributed OH reaction rate field for Case 3. It is essential to keep in mind that all of these fields were constructed from the *single* conserved scalar and scalar dissipation rate plane in Fig. 1 via the SDRL formulation. The differences evident among the three cases result entirely from the uniform rescaling of the scalar dissipation fields for the three flow conditions. Evidently the SDRL formulation allows the transition from thin "flamelet-like" fields near chemical equilibrium to broad "distributed" fields for large equilibrium departures with no need to explicitly distinguish between these two combustion environments, and without any need for separate models for treating them.

Figures 7-9 compare the OH mass fraction fields obtained from the SDRL formulation throughout the entire length of the flame for each of the three cases in Fig. 2. In each case the fields are shown at four different downstream locations relative to the mean flame length  $L$ , centered at  $x/L = 0.25, 0.50, 0.75$  and  $1.0$ . The size of each panel has been correctly scaled and placed for its downstream location to give a proper indication of the structure of the flame.

Differences evident in the OH concentration fields when comparing panels at the same downstream location for the three cases shown are due solely to the differing degrees of nonequilibrium. However, changes in the OH mass fraction fields among panels corresponding to differing  $x/L$  values for the same case reflect changes in both the depth of nonequilibrium as well as changes in the scalar and dissipation rate values with increasing downstream location in the flame. For the jet similarity scalings, the scalar field values decrease with increasing distance from the jet source as  $\zeta \sim x^{-1}$ . Coupled with the linear increase in all length scales in the jet with increasing  $x$ , the resulting scalar dissipation field values decrease with distance from the jet source like  $\nabla\zeta \cdot \nabla\zeta \sim x^{-4}$ . Thus, in examining these results, it must be kept in mind that comparisons made among different cases but at the same  $x/L$  location show the effects of the degree of nonequilibrium only, while comparisons made at different downstream locations within the same case demonstrate the effects of both nonequilibrium level and changes in the scalar field values. Arranging the results as shown in Figs. 7-9 allows separating the changes resulting solely from the degree of nonequilibrium from those resulting from changes in the conserved scalar and dissipation rate values. Table 1 gives the relative strain rates in each panel.

Note that the features of the resulting OH fields in Figs. 7-9 look very similar to those in direct OH PLIF imaging measurements in turbulent jet flames under varying degrees of chemical nonequilibrium [19, 20]. This is all the more striking in view of the fact that, despite the wide variations in the OH concentration field structure seen in these results with changing downstream position and with increasing depth of nonequilibrium among the three cases considered, all of these fields ultimately resulted from the same conserved scalar data plane shown in Fig. 1. Thus thin "flamelet-like" OH mass fractions and reaction rates at small  $x/L$  in Case 1, and the broad "distributed" regions of high OH concentrations and reaction rates in Case 3, all resulted from a simple layer-like structure in the scalar dissipation rate field in Fig. 1b and all can be reconciled with the single physically-based formulation given in §3 for these strained dissipation and reaction layers.

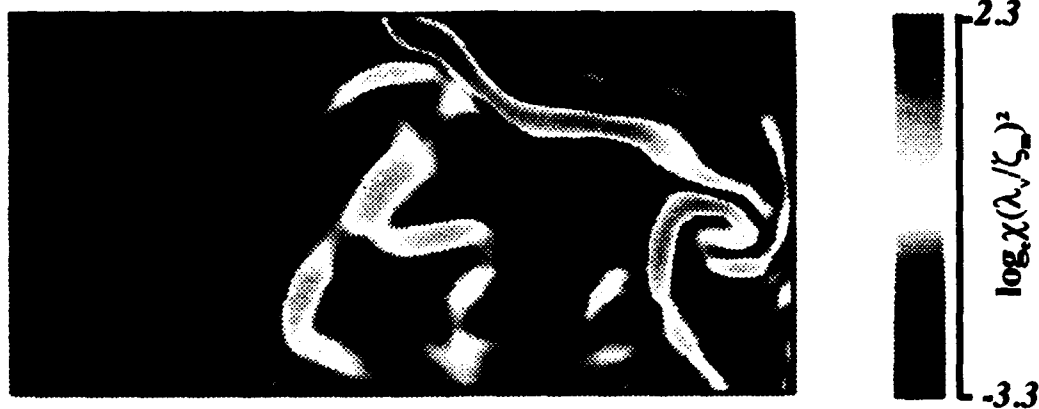
**1.2.4 Summary.** The strained dissipation and reaction layer formulation introduced here provides a novel physically-based method for relating the

chemical state of nonequilibrium combustion in turbulent flows to the mixing state of one or more conserved scalars. The approach is motivated entirely by the locally one-dimensional dissipation layers seen to result from the dynamics of scalar mixing in turbulent flows. The fact that these dissipation layers are independent of the extent of chemical nonequilibrium in the flow indicates a locally one-dimensional structure in the underlying chemical species fields. The resulting strained dissipation and reaction layer model has certain resemblances to the classical "flamelet" model, but is based on entirely different physical observations, is derived from entirely different arguments, and is limited by an entirely different and more widely applicable set of conditions. Moreover, the local boundary conditions for solution of the local chemical state differ fundamentally from those in flamelet models.

Results obtained when this strained dissipation and reaction layer formulation is applied to imaging measurements of conserved scalar fields in turbulent flows, for conditions ranging from near equilibrium to deep nonequilibrium, demonstrate remarkable resemblances with direct PLIF imaging measurements of chemical species under similar combustion conditions. Notably, the present SDRL formulation inherently produces results showing a predominance of thin (flamelet) mass fraction and reaction rate fields under conditions of relatively weak chemical nonequilibrium, and the natural emergence and dominance of broad (distributed) species concentration and reaction rate fields for increasing equilibrium departures. This formulation thus provides a physical and theoretical framework that reconciles these two widely disparate views of the coupling of the underlying fluid dynamics to the reaction chemistry in turbulent combustion within a single model. The ubiquitous layer-like scalar dissipation structures seen in Fig. 1, together with this strained dissipation and reaction layer formulation, suffice to unify both the "flamelet" and "distributed" combustion regimes under differing conditions of nonequilibrium and locations in the flame.



(a)



(b)

Fig. 1. Scalar mixing measurements for a  $Sc \approx 1$  conserved scalar field, obtained in the self-similar far field of an axisymmetric turbulent jet at  $Re_\delta \approx 14,000$ , from [4]. (a) The conserved scalar field  $\zeta(x,t)$ . (b) The associated two-dimensional scalar dissipation rate field  $\log_e \chi(x,t)$ . Note that essentially all of the scalar dissipation field is organized into locally one-dimensional layer-like structures being stretched and folded by the underlying velocity gradient field.

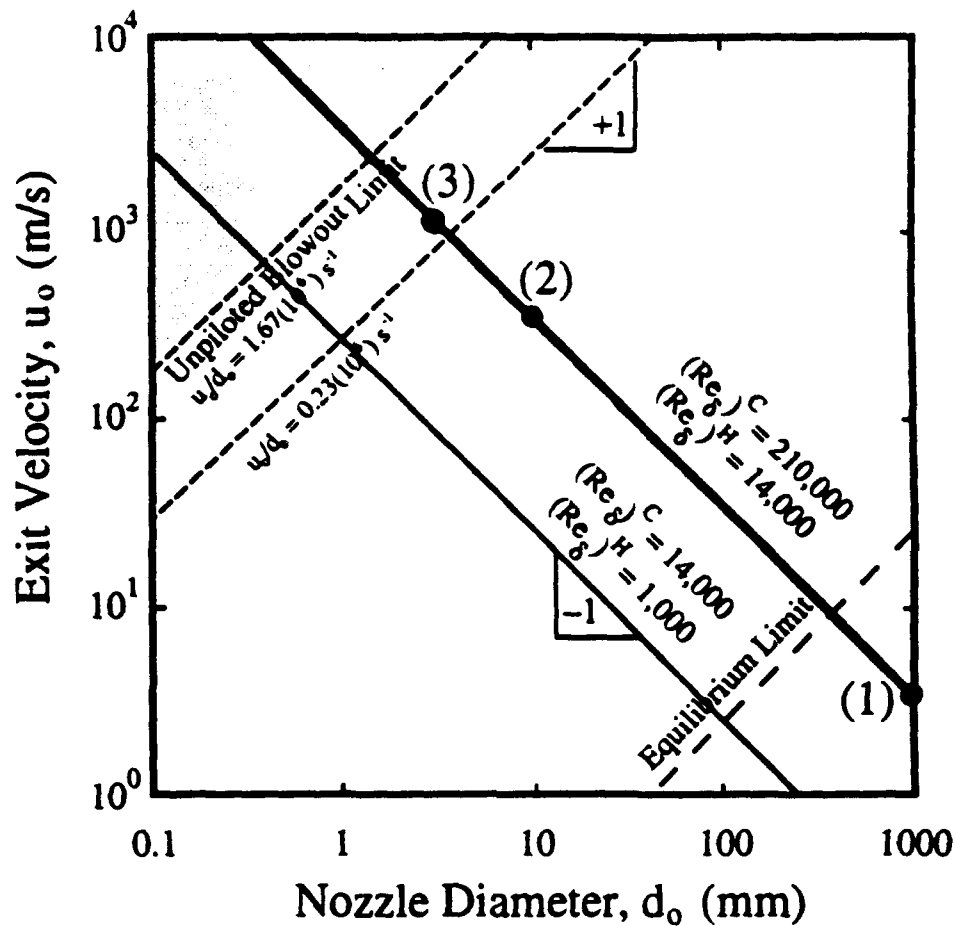


Fig. 2. Source conditions for turbulent hydrogen-air jet diffusion flames, showing depth of chemical nonequilibrium relative to the unpiloted blowout limit, given by  $u_o/d_o = 1.67 \cdot 10^6 s^{-1}$ . Solid line denotes conditions giving far-field hot flow Reynolds number  $Re = 14,000$  corresponding to cold flow  $Re = 210,000$ . Dashed lines denote constant global Damköhler number ( $u_o/d_o = \text{const.}$ ) Shown are the conditions for three cases, giving (Case 1) the equilibrium limit, (Case 2) moderate nonequilibrium, and (Case 3) deep nonequilibrium.

$x/L = 0.25$

*Case 1*



*Case 2*



*Case 3*



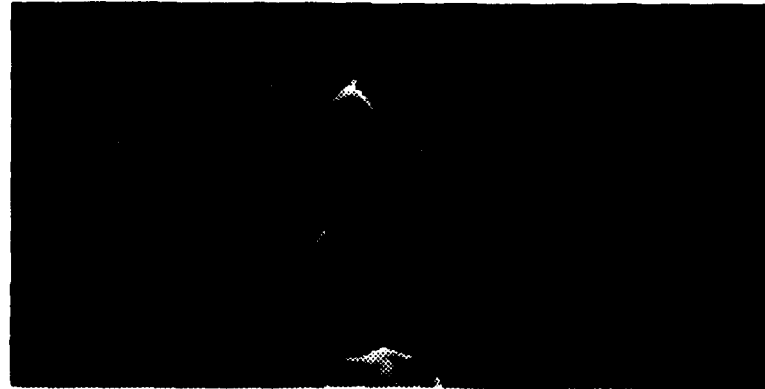
Fig. 3. Strained diffusion and reaction layer (SDRL) model results for OH mass fraction field  $Y_{OH}(x,t)$  in a hydrogen-air turbulent diffusion flame at  $x/L = 0.25$  for Case 1 (top), Case 2 (middle), and Case 3 (bottom), from the scalar mixing measurements in Fig. 1. Note the progression from thin "flamelet-like" OH zones near equilibrium, to broad "distributed" OH zones with increasing depth of chemical nonequilibrium.

$$x/L = 0.25$$

*Case 1*



*Case 2*



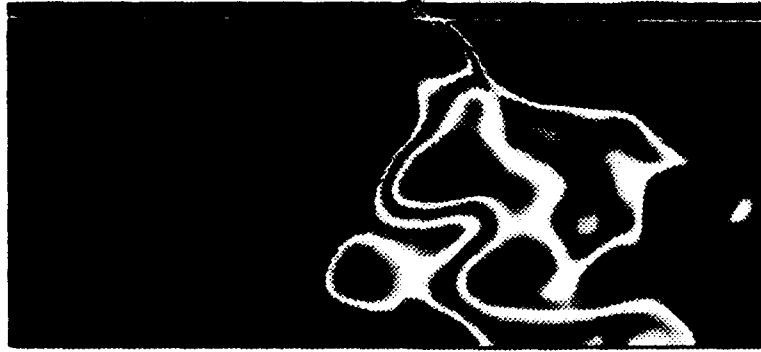
*Case 3*



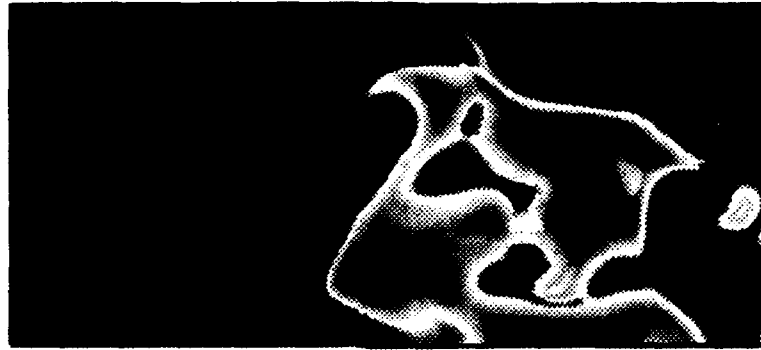
Fig. 4. Strained diffusion and reaction layer (SDRL) model results for OH reaction rate field  $w_{OH}(x,t)$  in a hydrogen-air turbulent diffusion flame at  $x/L = 0.25$  for Case 1 (top), Case 2 (middle), and Case 3 (bottom), from the scalar mixing measurements in Fig. 1. Note the broadening of the initially thin and layer-like OH reaction rate zones near equilibrium to relatively broad and diffuse OH reaction zones under conditions of deep chemical nonequilibrium.

$$x/L = 0.50$$

*Case 1*



*Case 2*



*Case 3*



Fig. 5. Strained diffusion and reaction layer (SDRL) model results for OH mass fraction field  $Y_{OH}(x,t)$  in a hydrogen-air turbulent diffusion flame at  $x/L = 0.50$  for Case 1 (top), Case 2 (middle), and Case 3 (bottom), from the scalar mixing measurements in Fig. 1. Compare with Fig. 3 to see effect of varying scalar values with ownstream position. Note the progression from thin "flamelet-like" OH zones near equilibrium, to broad "distributed" OH zones with increasing depth of chemical nonequilibrium.

$x/L = 0.50$

*Case 1*



*Case 2*



*Case 3*



Fig. 6. Strained diffusion and reaction layer (SDRL) model results for OH reaction rate field  $w_{OH}(x,t)$  in a hydrogen-air turbulent diffusion flame at  $x/L = 0.50$  for Case 1 (top), Case 2 (middle), and Case 3 (bottom), from the scalar mixing measurements in Fig. 1. Compare with Fig. 4 to see effect of varying scalar values with downstream position. Note the dramatic broadening of the initially thin and layer-like OH reaction rate zones near equilibrium into fully broad and diffuse OH reaction zones under conditions of deep chemical nonequilibrium.

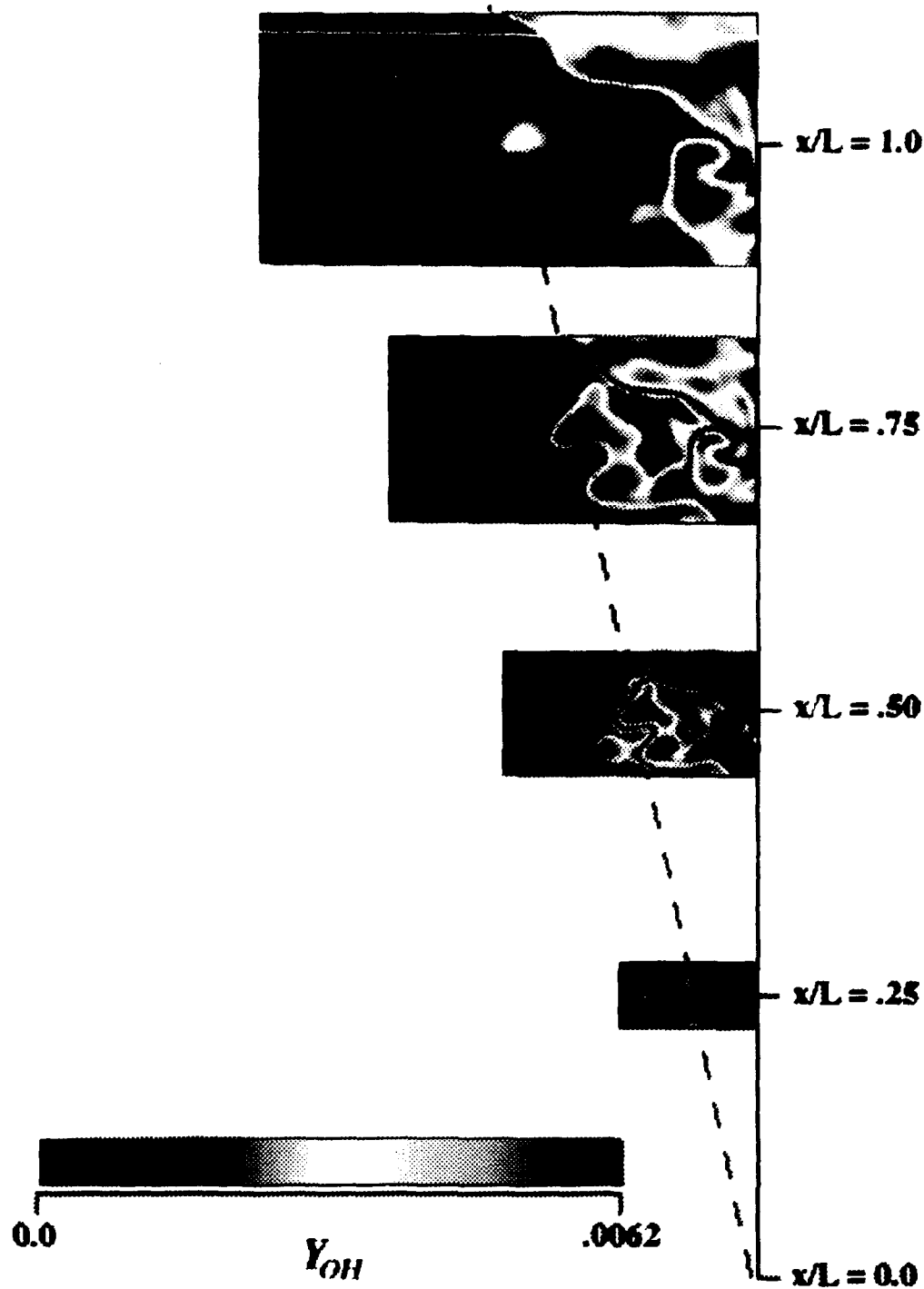


Fig. 7. Stained diffusion and reaction layer (SDRL) model results for composite OH mass fraction field  $Y_{OH}(x,t)$  in a hydrogen-air turbulent diffusion flame near equilibrium (Case 1) at four downstream locations:  $x/L = 0.25, 0.50, 0.75$  and  $1.0$ . Compare with Figs. 8 and 9 to see effect of varying global Damköhler number. See Table 1 for relative strain rate values. Note the progression from thin layer-like OH zones near the nozzle exit, to increasingly broader OH zones as the flame tip is approached.

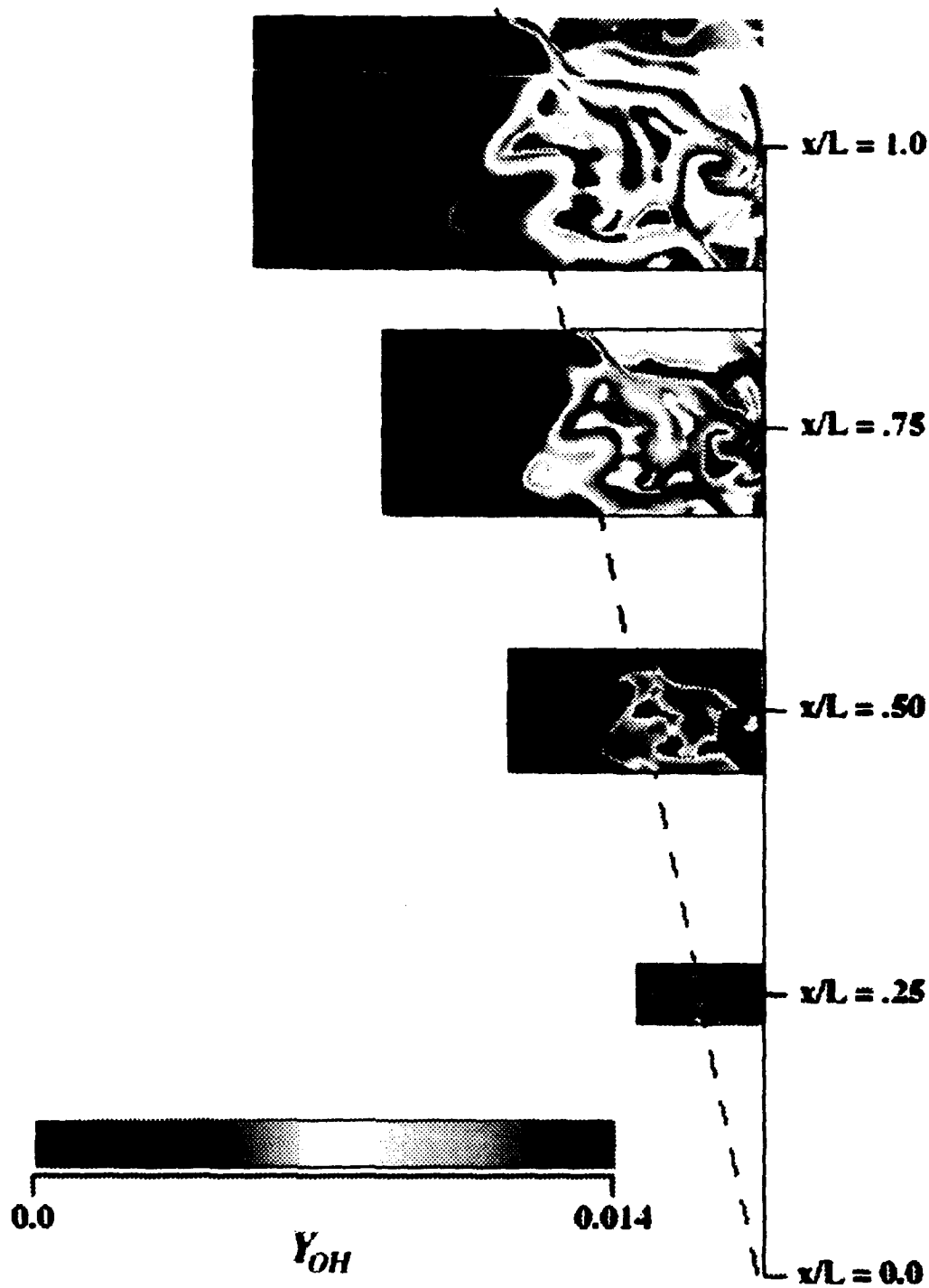


Fig. 8. Strained diffusion and reaction layer (SDRL) model results for composite OH mass fraction field  $Y_{OH}(x,t)$  in a hydrogen-air turbulent diffusion flame at moderate nonequilibrium conditions (Case 2) at four downstream locations:  $x/L = 0.25, 0.50, 0.75$  and  $1.0$ . Compare with Figs. 7 and 9 to see effect of varying global Damköhler number. See Table 1 for relative strain rate values. Note the broadening of the OH zones relative to Case 1 in Fig. 7.

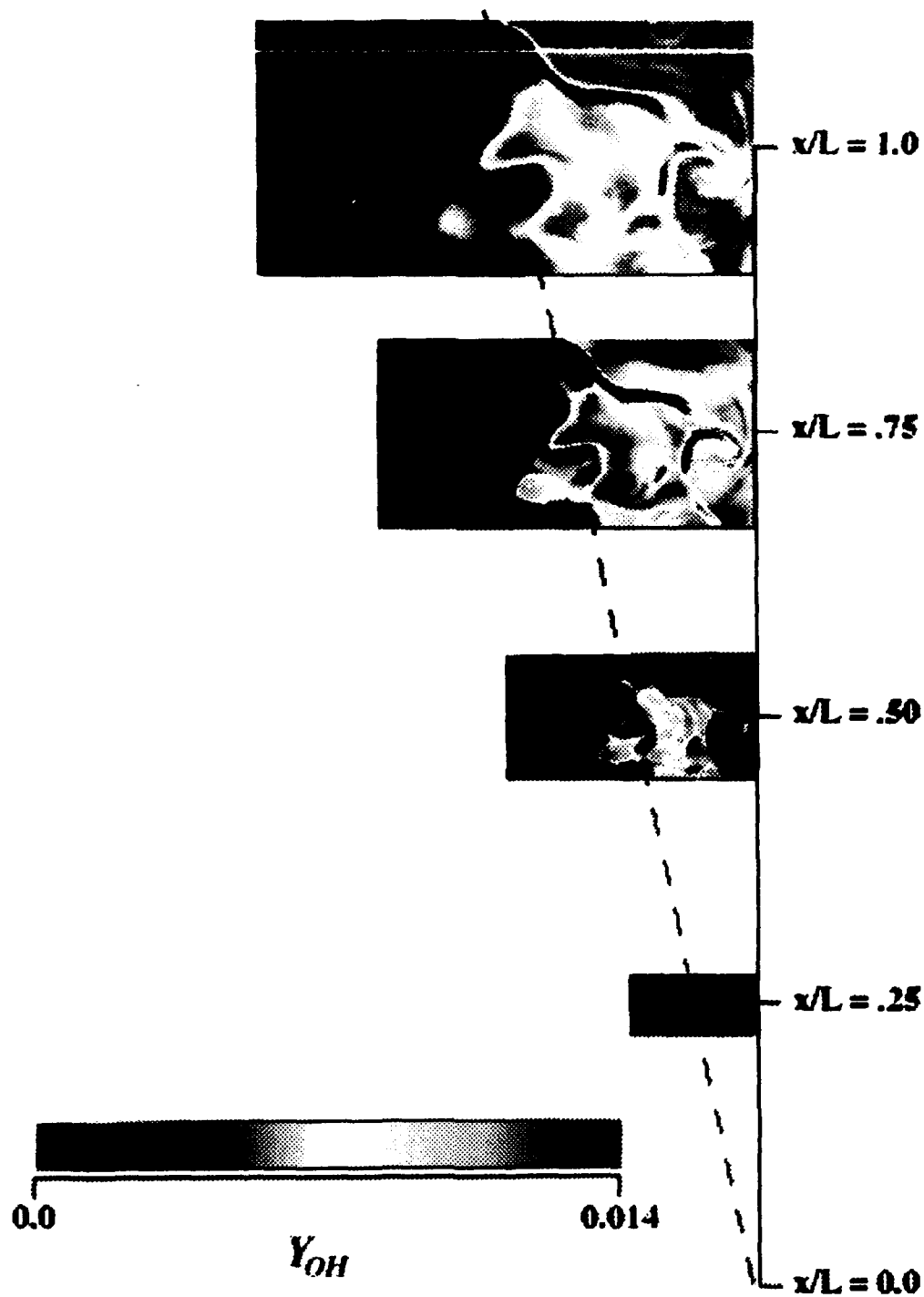


Fig. 9. Stained diffusion and reaction layer (SDRL) model results for composite OH mass fraction field  $Y_{OH}(x,t)$  in a hydrogen-air turbulent diffusion flame at deep nonequilibrium conditions (Case 3) at four downstream locations:  $x/L = 0.25, 0.50, 0.75$  and  $1.0$ . Compare with Figs. 7 and 8 to see effect of varying global Damköhler number. See Table 1 for relative strain rate values.

### 1.3. Topology and Scaling Properties of Scalar Dissipation Layers

The model described in §1.2 related the local state of chemical reactions to the mixing state of one or more conserved scalars in a turbulent reacting flow, based on the observation from our previous work that essentially all the scalar dissipation is concentrated in simple, locally one-dimensional, sheet-like structures. A complete model for turbulent reacting flow then also requires a means for predicting the topology of these sheet-like structures in a given turbulent flow in order to describe the local molecular mixing state. It is known that the quasi-deterministic large scale structures in a turbulent flow control the entrainment properties of the flow, and that these large structures differ from one flow to another. At the same time, it is believed that the structure and dynamics of the small scales in fully-developed turbulent flows are quasi-universal, satisfying Reynolds number asymptotics and displaying certain universal statistical scaling properties. However, it is only recently that the fully three-dimensional, time-varying, small scale structure of mixing in turbulent flows have been accessible to direct experimental study (see our previous AFOSR Reports). An example of such a measurement is shown in Fig. 1, where the concentration field  $\zeta(\mathbf{x}, t)$  of a dynamically passive, conserved scalar quantity being mixed by the underlying turbulent flow is shown in a small volume element of the flow. The mixing of such a scalar can be quantified in terms of the scalar energy dissipation rate field  $(ReSc)^{-1} \nabla \zeta \cdot \nabla \zeta(\mathbf{x}, t)$ , also shown for the same volume element in Fig. 1. Of primary interest for the present purposes are the highly folded sheet-like structures into which the scalar dissipation field is formed by the underlying three-dimensional time-varying turbulent flow field.

The detailed structure of the mixing patterns that result from the repeated stretching, reorientation, and folding of scalar dissipation layers by time-varying flows have been previously discussed in terms of the striation thickness distribution (STD). The STD is, however, notoriously difficult to measure. Consequently, owing to the inherently sheet-like structure of the scalar dissipation field, we will compare the distribution of dissipation layer separations. The procedure we use for determining these distributions is described below.

**1.3.1 Algorithms** Determining the dissipation layer separation distribution first requires that the set of points containing the dissipation layer centers must be found within each three-dimensional scalar dissipation volume from the turbulent flow experiments. We use an algorithm for automatically finding the dissipation layer centers, however as is often the case in "machine vision" applications, this is more difficult to do well than it might appear. Extensive tests conducted with various algorithms revealed features necessary for reliably identifying the layer centers in the algorithm that was finally used. This algorithm is based principally on the scalar gradient vector field  $\nabla\zeta(\mathbf{x},t)$ . Briefly, it begins by thresholding the gradient magnitude field (dissipation rate field) at some chosen level. Next, it identifies the edges of the regions in which the dissipation rate is above the threshold value. To do this, for each point the local unit normal vector for the layer is determined based on the local gradient vector information. The edges of the layer are then found by marching in both directions along this unit normal direction until one of two criteria are met: (i) the scalar dissipation at the candidate edge point drops below the chosen threshold level, or (ii) the dot product between the scalar gradient unit vector at the original point and that at the candidate edge point changes sign. The resulting edge locations for the dissipation layers are then used to identify candidate midpoints representing the dissipation layer centers. A further check is made among these candidate dissipation layer center points to insure single pixel thickness for the resulting surface before finally admitting a pixel to the set of layer center points.

**1.3.2 Test Cases** Figure 10 shows examples of the resulting dissipation layer centers identified by this algorithm for two data planes. Note that most of the layer centers are accurately determined, though there are instances where very weak dissipation layers produce either "holes" or "erroneous layers." Generally speaking, algorithms capable of reliably detecting very weak layers produce many erroneous layers. Conversely, attempts to reduce the number of erroneous layers tend to miss the weaker dissipation layers. The final algorithm used is a compromise between these two competing interests, representing roughly an "optimum" among the various identification strategies attempted. Tests conducted with synthetically generated surfaces having varying levels of imperfection verify that the resulting distribution of layer separations can be accurately obtained.

**1.3.3 Distributions** Probability densities of dissipation layer separations were computed for each of 29 individual three-dimensional  $256^3$  spatial data volumes of the type shown in Fig. 1 from our turbulent flow measurements at  $Re_\delta \approx 3700$ . These volumes were equally spaced in time, and spanned slightly more than 2.5 outer scale turn-over times ( $\delta/u$ ) of the flow. The size of each volume was roughly  $(2\lambda_v)^3$ , where  $(\lambda_v/\delta) \approx 11.2 \cdot Re_\delta^{-3/4}$  is the local strain-limited velocity gradient length scale in the turbulent flow, and  $Re_\delta \equiv (u\delta/\nu)$  is the local outer-scale Reynolds number based on the length and velocity scales  $\delta$  and  $u$  characterizing the local mean shear in the flow. The scalar field within any volume thus represents the signature of the mixing process at the small scales of the flow. The dissipation layer separation distribution resulting from ensemble statistics over the entire set of spatial data volumes is shown in Fig. 11. A roughly  $-3$  power law scaling can be seen in the distribution of layer separations over this range of length scales, reminiscent of the power-law scale-similarities typically found in high Reynolds number turbulent flows.

Although the ensemble-averaged distribution exhibits this  $-3$  power law scaling, the individual dissipation layer separation distributions vary considerably from one data volume to the next, as shown in Fig. 12. The  $-3$  scaling appears to result only from averaging over many such individual uncorrelated volumes, but is not evident in any single volume. However, while the distribution varies significantly at large layer separations, for small separations the results for all volumes are nearly the same. The distributions for small separations are essentially invariant and show a roughly lognormal scaling, while for large separations the distributions are very different. Ambient fluid is continually entrained into the turbulent mixing region, creating potentially large voids in the dissipation field which are subsequently broken down by the continual stretching and folding process. Thus it is possible that the large separations in the turbulent flow result principally from the remnants of this entrainment process. The  $-3$  scaling that results in the ensemble-averaged distribution in Fig. 12 would then be the result of some appropriately weighted average over the distribution of large voids created by the entrainment and subsequent breakdown ("cascade") process. At this stage, however, it is too early to assign a definitive explanation to this surprisingly simple scaling result.

**1.3.4 Spectra** Our examination of the dissipation layer separation distribution is motivated by the underlying layer-like topology of the scalar dissipation field in turbulent flows. The extent of this layered nature of turbulent mixing has only recently been appreciated. Classically, the mixing process has been interpreted principally in terms spectral decompositions of the scalar field. The folding of these dissipation layers evident, for example, in Fig. 1 then leads to predicted scalings at the high wavenumber end of the spectrum. For  $Sc \gg 1$ , a  $k^{-1}$  power law scaling was originally suggested by Batchelor. This scaling has been supported by measurements of Clay & Gibson, but has recently been brought into question by Miller & Dimotakis. These earlier measurements were all based on single-point time series data, interpreted through a Taylor hypothesis as one-dimensional spatial intersections. The three-dimensional spatial nature of our data allows the first direct examination of this classical prediction for turbulent mixing.

Figure 13 shows our results for the three-dimensional isotropic scalar spectrum function  $E(k)$ . The result is shown in both Kolmogorov (top) and Batchelor (bottom) coordinates. In the former, all spectra are classically expected to collapse in the inertial range, and the results for differing Schmidt numbers would separate at  $k = k_K$  into  $-1$  power law regions, whose extent would be proportional to  $Sc^{1/2}$ . In the latter, all spectra would collapse in the rolloff at the highest wavenumbers and in the presumed  $-1$  scaling region, and their inertial ranges would be shifted appropriately. It can be seen that, owing to the extremely high resolution of the present measurements and the short (256-point) spatial extent in any of the three spatial dimensions, these data just reach into the Batchelor range. At the lowest wavenumbers represented, the data appear to asymptote to the classical  $-1$  power law prediction, and are consistent with the one-dimensional spectra of Clay. However, the crossover among the power law regimes, and into the rolloff range, occurs at wavenumbers roughly an order of magnitude lower than suggested by the classical theory.

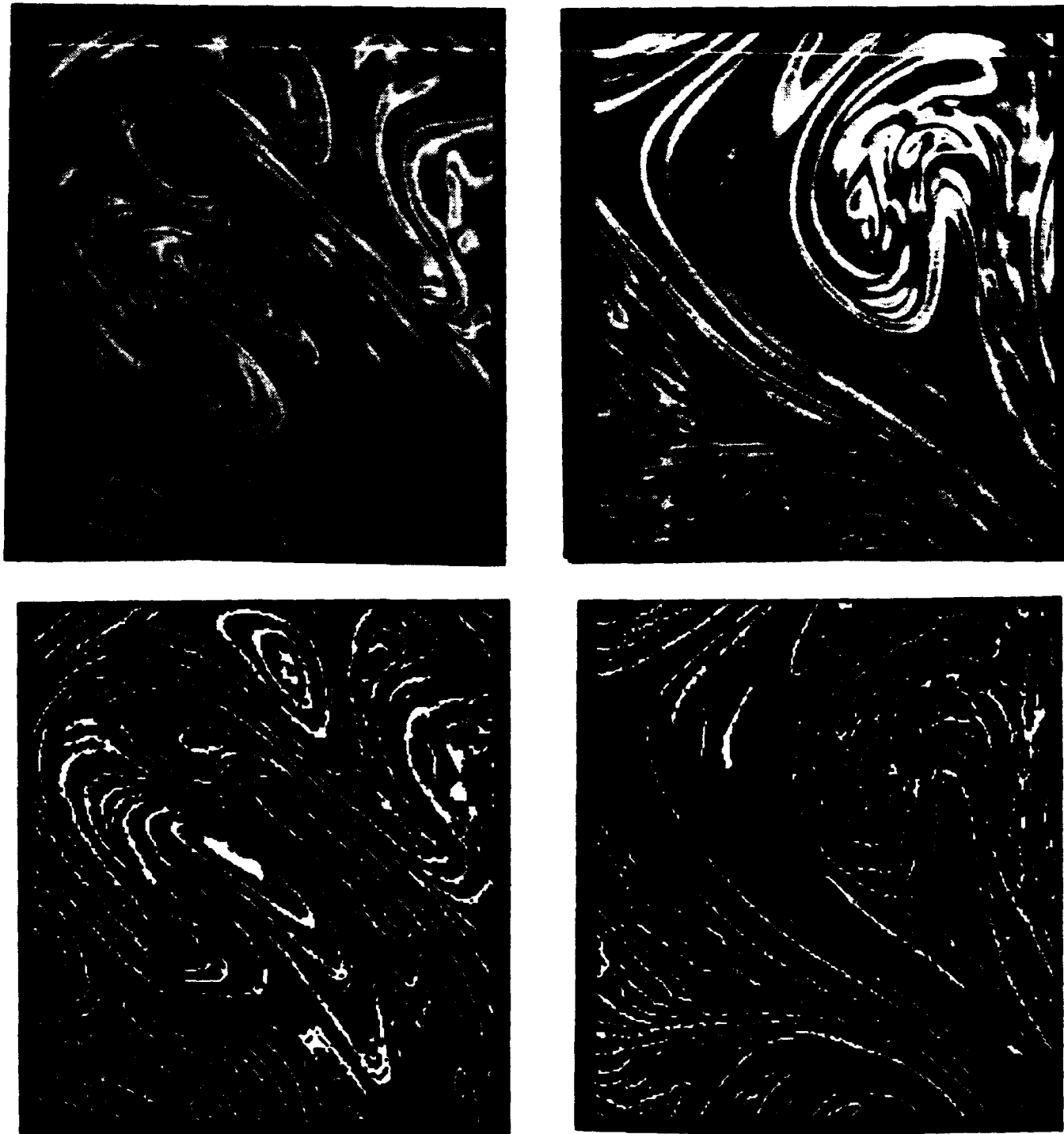


**Fig. 10.** Examples of the three-dimensional scalar energy dissipation rate field (top), displayed as two-dimensional cuts through two different data volumes, together with the corresponding intersection of the surface of dissipation layer centers. Note that the layer centers are accurately determined.

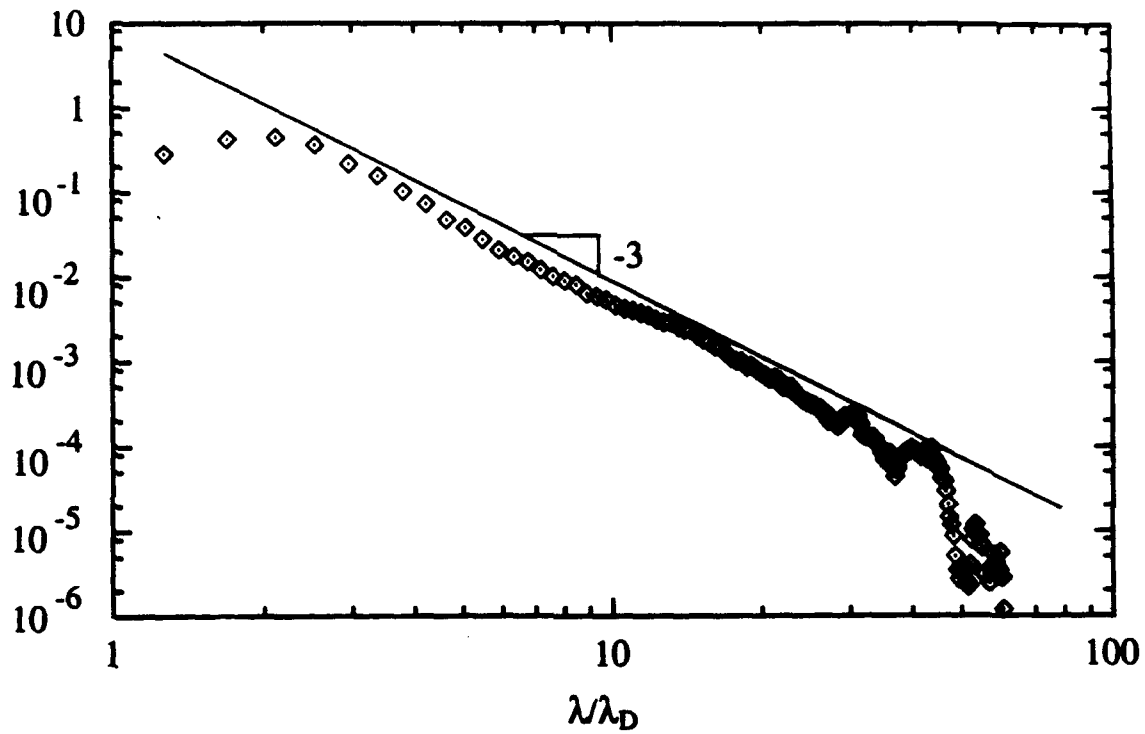


Fig. 11. Composite layer separation pdf for the fully three-dimensional turbulent shear flow data with  $Re = 3700$ . The probability density function is calculated from 29 temporally spaced volumes of which Fig. 1 is an example using the three-dimensional algorithm for finding scalar energy dissipation layer separation distances. Notice the prevalent  $-3$  slope covering nearly all range of separations in this log-log plot.

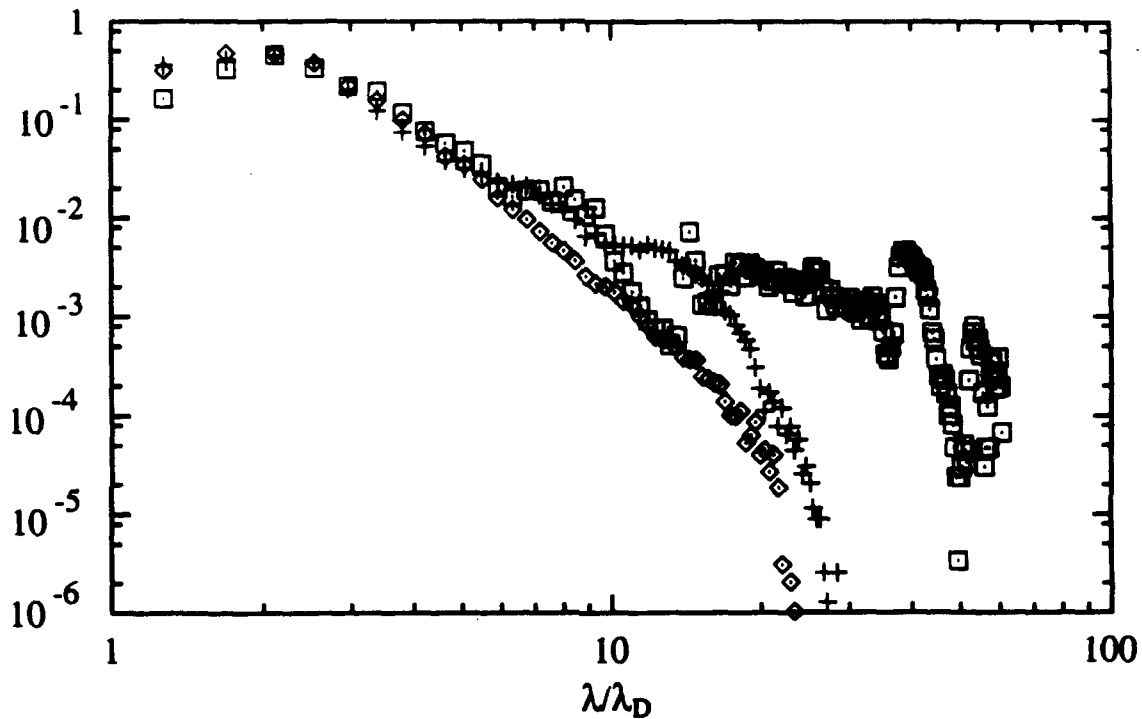


Fig. 12. Layer separation pdf's for three different volumes of the three-dimensional turbulent shear flow data of which Fig. 1 is an example. Notice how the pdf's match fairly well at small separations and can vary quite radically at large separations. This is simply consistent with the shape of the pdf which indicates that the statistics of the more prevalent smaller separation distances will settle down much faster than those of the more infrequent larger separations which will require a longer time average to obtain accurate results.

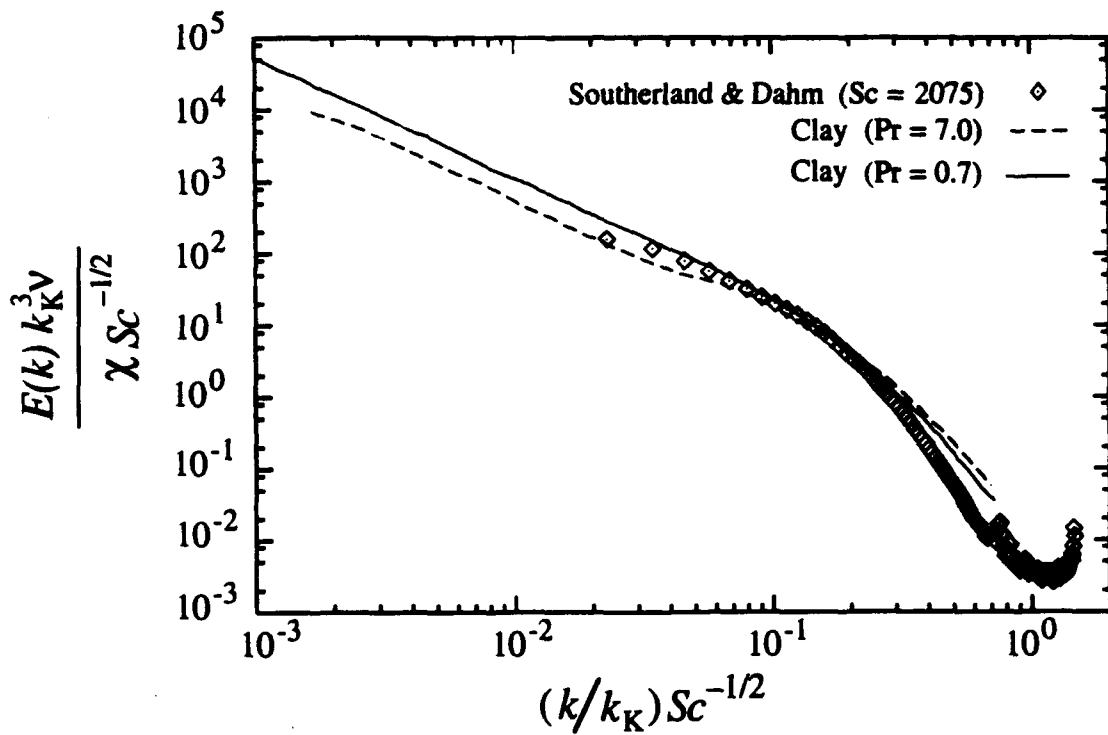
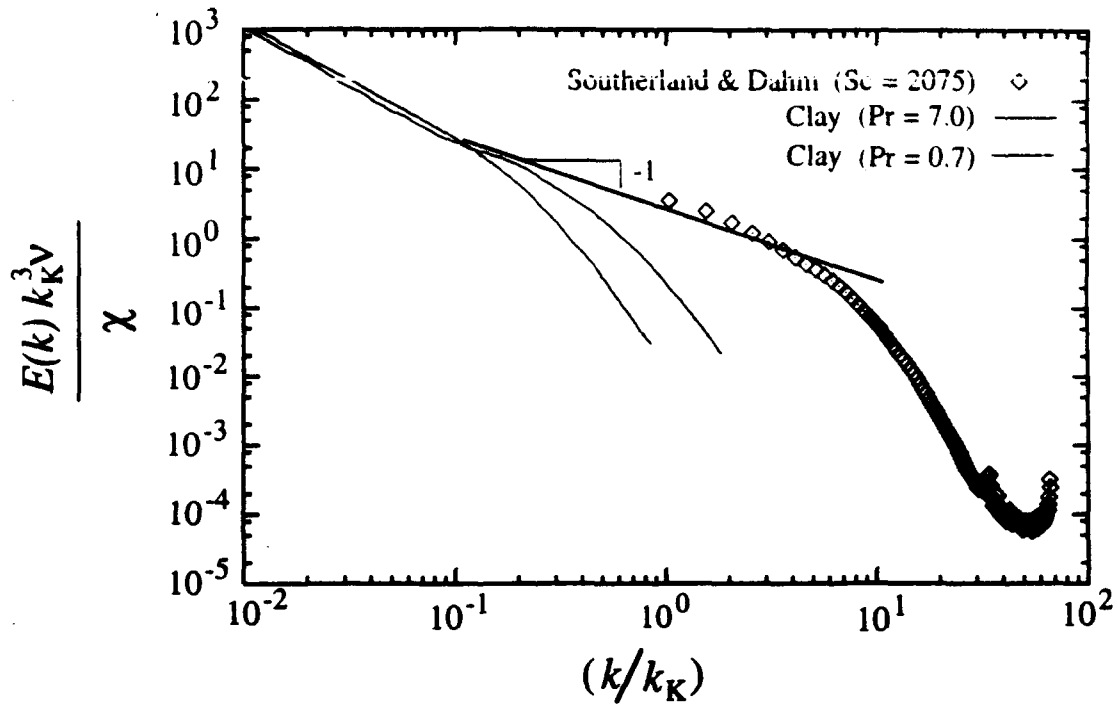


Fig. 13. High wavenumber scalar spectra obtained from three-dimensional  $Sc \gg 1$  measurements of the type shown in Fig. 1. Shown are results plotted in Kolmogorov coordinates (top) and Batchelor coordinates (bottom). Notice the asymptotic approach to the  $-1$  scaling in the Batchelor range, and the correlation in terms of Schmidt (Prandtl) number,

*References*

- [1] Dahm, W.J.A. & Buch, K.A. (1991) High resolution, three-dimensional ( $256^3$ ), spatio-temporal measurements of the conserved scalar field in turbulent shear flows; Turbulent Shear Flows 7, pp. 17-26, W.C. Reynolds, Ed., Springer Verlag, Berlin.
- [2] Dahm, W.J.A., Southerland, K.B. & Buch, K.A. (1991) Four-dimensional laser induced fluorescence measurements of conserved scalar mixing in turbulent flows; Applications of Laser Techniques to Fluid Mechanics, pp. 3-18, R. Adrian, Ed., Springer Verlag, Berlin.
- [3] Dahm, W.J.A., Southerland, K.B. & Buch, K.A. (1991) Direct, high resolution, four-dimensional measurements of the fine scale structure of  $Sc \gg 1$  molecular mixing in turbulent flows; *Phys. Fluids A* 3, 1115-1127.
- [4] Buch, W.J.A. & Dahm, W.J.A. (1992) Fine scale structure of conserved scalar mixing in turbulent shear flows:  $Sc \gg 1$ ,  $Sc = 1$  and implications for reacting flows; University of Michigan Report No. 026779-5, The University of Michigan, Ann Arbor, MI.
- [5] Buch, K.A., Dahm, W.J.A., Dibble, R.W. & Barlow, R.S. (1992) Equilibrium structure of reaction rate fields in turbulent diffusion flames; *Proc. 24th Symp. (Int'l.) on Comb.* 295-301, The Combustion Institute, Pittsburgh.
- [6] Dahm, W.J.A. & Bish, E.S. (1993) High resolution measurements of molecular transport and reaction processes in turbulent combustion; in Turbulence and Molecular Processes in Combustion, pp. 287-302, (T. Takeno, Ed.) Elsevier Science Publishers, Amsterdam.
- [7] Siggia, E.D. (1981) Numerical study of small scale intermittency in three-dimensional turbulence; *J. Fluid Mech.* 107, 375-406.
- [8] Kerr, R.M. (1985) Higher-order derivative correlations and the alignment of small scale structures in isotropic numerical turbulence; *J. Fluid Mech.* 153, 31-58.
- [9] Reutsch, G.R. & Maxey, M.R. (1991) Small-scale features of vorticity and passive scalar fields in homogeneous isotropic turbulence; *Phys. Fluids A* 3, 1587-1597.
- [10] Mell, W., Kosály, G. & Riley, J.J. (1993) An investigation of closure models for nonpremixed turbulent reacting flows; AIAA Paper No. 93-0104, AIAA, Washington, D.C.
- [11] Montgomery, C.J., Kosály, G. & Riley, J.J. (1993) Direct numerical simulation of turbulent  $H_2-O_2$  combustion using reduced chemistry; AIAA Paper No. 93-0248, AIAA, Washington, D.C.
- [12] Long, M.B. (1993) Proceedings of the 1993 AFOSR Contractors Meeting in Propulsion, AFOSR, Washington, D.C.; also private communication.

- [13] Peters, N. (1984) Laminar diffusion flamelet models in nonpremixed turbulent combustion. *Prog. Energy Combust. Sci.* 10, 319-339.
- [14] Williams, F. A., Combustion Theory, 2nd ed., Addison-Wesley, 1985.
- [15] Bilger, R.W. (1988) The structure of turbulent nonpremixed flames. *Proc. 22nd Symp. (Int'l.) on Comb.* 475-488, The Combustion Institute, Pittsburgh.
- [16] Chen, J.-Y. (1992) private communication.
- [17] Peters, N. (1986) Laminar flamelet concepts in turbulent combustion. *Proc. 21st Symp. (Int'l.) on Comb.* 1231-1250, The Combustion Institute, Pittsburgh.
- [18] Miller, J.A. & Bowman, C.T. (1989) Mechanism and modeling of nitrogen chemistry in combustion. *Prog. Energy Combust. Sci.* 15, 287-338.
- [19] Seitzman, J, Paul, P.H., Hanson, R.K. & Üngüt, A. (1990) AIAA Paper No. 90-0160, American Institute of Aeronautics and Astronautics, Washington, D.C.
- [20] Clemens, N.T., P.H. Paul & M.G. Mungal (1992) private communication.

## 2. Personnel

### A. Faculty

Dr. Werner J.A. Dahm; Associate Professor, The University of Michigan, Department of Aerospace Engineering, Ph.D., US Citizen.

### B. Graduate Students

Southerland, K.B.; Graduate Student, University of Michigan, Department of Aerospace Engineering, Ph.D. program, US Citizen. Mr. Southerland is the principal graduate student research assistant working on this grant, and he is fully supported through his work on the grant.

Bish, E.; The University of Michigan, Department of Aerospace Engineering, Ph.D. program, US Citizen. Mr. Bish is 85% supported through a DoEd Fellowship; he receives 15% support (\$200/month + 1 summer month) from his work on this grant.

Frederiksen, R.E.; The University of Michigan, Department of Aerospace Engineering, Ph.D. program, US Citizen. Mr. Frederiksen is 80% supported through a DoEd Fellowship; he receives 10% support (\$100/month + 1.5 summer months) from his work on this grant. Application to the DoD ASSERT Program has been made to allow him to work full-time on this project with funds outside the original grant budget.

### C. Post-Doctorates

None.

## 3. Publications

The following publications have resulted during this reporting period in part from the work undertaken in this research program into the structure of chemical reactions in turbulent flows.

1. Buch, K.A., Dahm, W.J.A., Dibble, R.W. & Barlow, R.S. (1992) Equilibrium structure of reaction rate fields in turbulent diffusion flames; Proceedings of the 24th (International) Symposium on Combustion, The Combustion Institute, Pittsburgh, pp. 295-301.
2. Dahm, W.J.A. and Bish (1993) High resolution measurements of molecular

- transport and reaction processes in turbulent combustion; in Turbulence and Molecular Processes in Combustion, pp. 287-302, (T. Takeno, Ed.) Elsevier Science Publishers B.V.
3. Everest, D., Driscoll, J.F., Dahm, W.J.A. & Feikema, D. (1993) Images of the 2D temperature field and temperature gradients to quantify thermal mixing rates within a non-premixed turbulent jet flame; Combustion and Flame, accepted for publication.
  4. Dahm, W.J.A., Tryggvason, G. & Zhuang, M.M. (1993) Integral method solution of time-dependent strained diffusion-reaction equations with multi-step kinetics; SIAM Journal of Applied Mathematics, submitted.
  5. Southerland, K.B., Frederiksen, R.D., Dahm, W.J.A. & Dowling, D.R. (1993) Comparisons of mixing in chaotic and turbulent flows; Chaos, Solitons & Fractals, submitted.
  6. Bish, E.S. & Dahm, W.J.A. (1993) Strained dissipation and reaction layer analyses of nonequilibrium chemistry in turbulent reacting flows; submitted to 25th International Symposium on Combustion, The Combustion Institute, Pittsburgh.
  7. Bish, E.S. & Dahm, W.J.A. (1993) Non-equilibrium structure of H<sub>2</sub>-Air combustion in turbulent jets; AIAA Paper No. 94-0100, 32nd AIAA Aerospace Sciences Mtg, January 10-14, 1994, Reno, NV.
  8. Suresh, N.C., Dahm, W.J.A. & Tryggvason, G. (1993) LIM computations of chemical reactions in spatially and temporally developing shear flows; AIAA Paper No. 94-0870, 32nd AIAA Aerospace Sciences Mtg, January 10-14, 1994, Reno, NV.
  9. Bish, E.S. & Dahm, W.J.A. (1993) Strained dissipation and reaction layer analyses of turbulent reacting flows; submitted for the 25th AIAA Fluid Dynamics Conference, June 20-23, 1994, Colorado Springs, CO.
  10. Southerland, K.B. & Dahm, W.J.A. (1993) A structural and spectral study of fine-scale mixing in turbulent flows; submitted for the 25th AIAA Fluid Dynamics Conference, June 20-23, 1994, Colorado Springs, CO.

#### 4. Presentations

The following presentations have resulted during this reporting period in part from the research work undertaken in this research program into the structure of chemical reactions in turbulent flows.

1. Micromasurements of Fluid Turbulence – Invited Plenary Lecture, 46th Annual

- Meeting, Division of Fluid Dynamics, American Physical Society, Tempe, AZ, November 1993, abstract in Bull. Am. Phys. Soc., Vol. 38, No. 12, 2255.
2. Conserved Scalar Imaging in Turbulent Diffusion Flames – Invited Presentation, 22nd Meeting of the Sandia Technical Group on Aerothermochemistry of Reacting Flows, Sandia National Laboratories, Livermore, CA, October 1993.
  3. A Strained Dissipation and Reaction Layer Formulation for Turbulent Diffusion Flames; Paper No. 93-063, 1993 Fall Meeting of the Western States Section of the Combustion Institute, Menlo Park, CA, October 1993.
  4. Striation Thickness Distributions in Turbulent Flows – 46th Annual Meeting, Division of Fluid Dynamics, American Physical Society, Albuquerque, NM, November 1993; abstract in Bull. Am. Phys. Soc., Vol. 38, No. 12, 2205.
  5. A Strained Dissipation and Reaction Layer Formulation for Turbulent Reactive Flows – 46th Annual Meeting, Division of Fluid Dynamics, American Physical Society, Albuquerque, NM, November 1993; abstract in Bull. Am. Phys. Soc., Vol. 38, No. 12, 2269.
  6. Comparison of Fractal Properties in Chaotically Advected and Turbulent Flows – 46th Annual Meeting, Division of Fluid Dynamics, American Physical Society, Albuquerque, NM, November 1993; abstract in Bull. Am. Phys. Soc., Vol. 38, No. 12, 2194.
  7. Microstructure of Turbulence and Turbulent Reacting Flows – Invited Seminar, Mechanical Engineering Department, University of Washington, Seattle, WA, April 1993.

## **5. Research-Related Interactions**

Interactions based on research results emanating from this work have been initiated with G. Kosály at U. Washington, T. Poinot at CERFACS in France, and W. Kollmann at UC-Davis.

## **6. Summary of Inventions**

No invention disclosures are to be filed on the basis of work done during this reporting period.